Acta Crystallographica Section F
Structural Biology and Crystallization Communications
ISSN 1744-3091

Crystallization of recombinant bifunctional nuclease TBN1 from tomato

Tomáš Koval',[a,b]* Petra Lipovová,[c] Tomáš Podzimek,[c,d] Jaroslav Matoušek,[d] Jarmila Dušková,[e] Tereza Skálová,[e] Andrea Štěpánková,[e] Jindřich Hašek[e] and Jan Dohnálek[a]

[a]Institute of Physics AS CR, v.v.i., Na Slovance 2, 182 21 Praha 8, Czech Republic, [b]Faculty of Mathematics and Physics, Charles University in Prague, Ke Karlovu 3, 121 16 Praha 2, Czech Republic, [c]Institute of Chemical Technology, Technická 5, 166 28 Praha 6, Czech Republic, [d]Institute of Plant Molecular Biology, Biology Centre AS CR, v.v.i., Branišovská 31, 370 05 České Budějovice, Czech Republic, and [e]Institute of Macromolecular Chemistry AS CR, v.v.i., Heyrovského nám. 2, 162 06 Praha 6, Czech Republic

Correspondence e-mail: koval.tomas@gmail.com

Received 9 September 2010
Accepted 18 November 2010

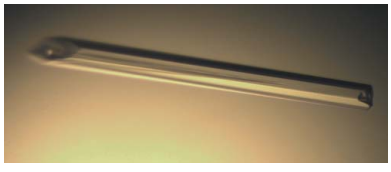

The endonuclease TBN1 from *Solanum lycopersicum* (tomato) was expressed in *Nicotiana benthamiana* leaves and purified with suitable quality and in suitable quantities for crystallization experiments. Two crystal forms (orthorhombic and rhombohedral) were obtained and X-ray diffraction experiments were performed. The presence of natively bound Zn^{2+} ions was confirmed by X-ray fluorescence and by an absorption-edge scan. X-ray diffraction data were collected from the orthorhombic (resolution of 5.2 Å) and rhombohedral (best resolution of 3.2 Å) crystal forms. SAD, MAD and MR methods were applied for solution of the phase problem, with partial success. TBN1 contains three Zn^{2+} ions in a similar spatial arrangement to that observed in nuclease P1 from *Penicillium citrinum*.

1. Introduction

Tomato endonuclease TBN1 from *Solanum lycopersicum* is a Zn^{2+}-dependent plant glycoprotein composed of 277 amino acids with a molecular mass of 31.6 kDa (about 37 kDa when fully glycosylated). It belongs to the plant nuclease I group (UniProt sequence accession No. Q0KFV0; gene name *tbn*1; Matoušek *et al.*, 2007). Nuclease I proteins are Zn^{2+}-dependent, Mg^{2+}-dependent or Ca^{2+}-dependent and are capable of cleaving both RNA and DNA in single-stranded and double-stranded forms, with a preference for bonds adjacent to adenine. They produce 5′-mononucleotides as end products in the pH range 5.0–6.5. They are EDTA-sensitive and their molecular weight is in the range 31–35 kDa. Important features of enzymes from this family are their ability to cleave different homopolymers and also their relation to fungal P1 and S1 nucleases (Pérez-Amador *et al.*, 2000). It has been shown that TBN1 plays a significant role in specific apoptotic functions and in plant tissue differentiation, vascular-system development and viroid pathogenesis (Matoušek *et al.*, 2007). The closest related nuclease of known structure is P1 nuclease from *Penicillium citrinum* (Romier *et al.*, 1998; PDB entry 1ak0), which has 28% sequence identity. It is known that some ribonucleases from animals and fungi, such as bovine pancreatic ribonuclease (RNase A), bovine seminal ribonuclease (BS-RNase), onconase and α-sarcin, have potent anticancer activity (Ledoux, 1955; Aleksandrowicz, 1958; Hosokawa & Irie, 1971; D'Alessio *et al.*, 1972; Dostál & Matoušek, 1972; Darzynkiewicz *et al.*, 1988; Ardelt *et al.*, 1991; Olson *et al.*, 1965). Many nucleases from the plant nuclease I family have similar structural features to animal ribonucleases (Green, 1994; Gite & Shankar, 1995; Chang & Gallie, 1997; Dangl *et al.*, 2000). Recently, anti-carcinogenic effects have also been demonstrated for nucleases from the plant nuclease I family, such as mung bean sprout nuclease I (Soucek *et al.*, 2006), extracellular nuclease I from black pine pollen (Lipovova *et al.*, 2008), recombinant HBN1 nuclease from *Humulus lupulus* and recombinant TBN1 nuclease (R-TBN1; Matousek *et al.*, 2008, 2009, 2010), but very little is known about the exact mechanisms of activity of these potent enzymes. The structure of R-TBN1 is

expected to help in better understanding the differences between animal/fungal and plant nucleases and their mechanisms of activity. It will provide new insights that will be useful for the development of anticancer and antiviral treatments involving the application of nucleases.

2. Materials and methods

2.1. Expression and purification

For crystallization and diffraction experiments, recombinant tomato nuclease (R-TBN1) was used. The protein was prepared by insertion of cDNA into the plant expression vector pLV07 and using *Agrobacterium tumefaciens* leaf disc infiltration and expression in *Nicotiana benthamiana* leaves (Matousek *et al.*, 2010). R-TBN1 was purified using ammonium sulfate precipitation, ion-exchange chromatography using a HiTrap Q FF column (Amersham), affinity chromatography on HiTrap Heparin HP (Amersham) and desalting on a PD-10 column (Amersham). The details of the procedure have been described previously by Lipovova *et al.* (2008) and Matousek *et al.* (2009).

2.2. Crystallization

For crystallization experiments, enzyme stored in 50 m*M* Tris–HCl pH 7.5 with the addition of 0.3 *M* NaCl was used. Initial screening was performed by the hanging-drop vapour-diffusion method using the 96-condition Index screen from Hampton Research (D'Arcy *et al.*, 2003) at 291 K with a protein concentration of 4 mg ml^{-1} and with a 1:1 volume ratio of reservoir to protein solution in the drop (0.5 + 0.5 µl). Crystals grew in 30 different conditions, mainly in the form of small needles, within 3–10 d. The optimization process for the most promising conditions (Index condition Nos. 46 and 85) included changes in pH, temperature and the concentrations of salts and polymers, seeding experiments, the application of the microbatch method, changes in protein concentration, changes in drop volume ratio and additive screening using Hampton Research Additive Screen (Cudney *et al.*, 1994). Crystals suitable for diffraction analysis were obtained as a result of optimization.

Table 1
Optimized crystallization conditions yielding crystals of R-TBN1 suitable for X-ray diffraction analysis.

No.	Precipitant solution	Method	Growth time	Typical crystal dimensions (µm)
1	0.18 *M* $MgCl_2$, 0.08 *M* Tris–HCl pH 8.5, 19%(*w*/*v*) PEG 3350	Hanging-drop vapour diffusion	3 d	500 × 70 × 70
2	0.1 *M* bis-tris pH 6.5, 10%(*w*/*v*) PEG MME 5000, 4%(*v*/*v*) DMSO	Hanging-drop vapour diffusion	1 week	1500 × 100 × 100
3	0.1 *M* bis-tris pH 6.5, 10%(*w*/*v*) PEG MME 5000, 0.48 *M* hexane-1,6-diol	Hanging-drop vapour diffusion	1 week	1500 × 100 × 100
4	0.1 *M* bis-tris pH 6.5, 10%(*w*/*v*) PEG MME 5000, 2%(*v*/*v*) butane-2,3-diol	Microbatch under paraffin oil	1 week	500 × 70 × 70

Four optimized crystallization conditions yielded crystals that were suitable for X-ray diffraction analysis. The first condition originated from Index condition No. 85. The hanging-drop vapour-diffusion method was used and the reservoir composition was 0.18 *M* magnesium chloride, 0.08 *M* Tris–HCl pH 8.5 and 19%(*w*/*v*) PEG 3350. The drop was formed by mixing 0.5 µl protein solution (at a concentration of 4 mg ml^{-1}) with 1.0 µl reservoir solution and the best crystals (of approximate dimensions 500 × 70 × 70 µm) were obtained using microseeding (Fig. 1*a*). The second condition originated from Index condition No. 46. The same method was used, with reservoir composed of 0.1 *M* bis-tris pH 6.5, 10%(*w*/*v*) PEG monomethyl ether 5000 (PEG MME 5000) and 4%(*v*/*v*) dimethyl sulfoxide (DMSO).

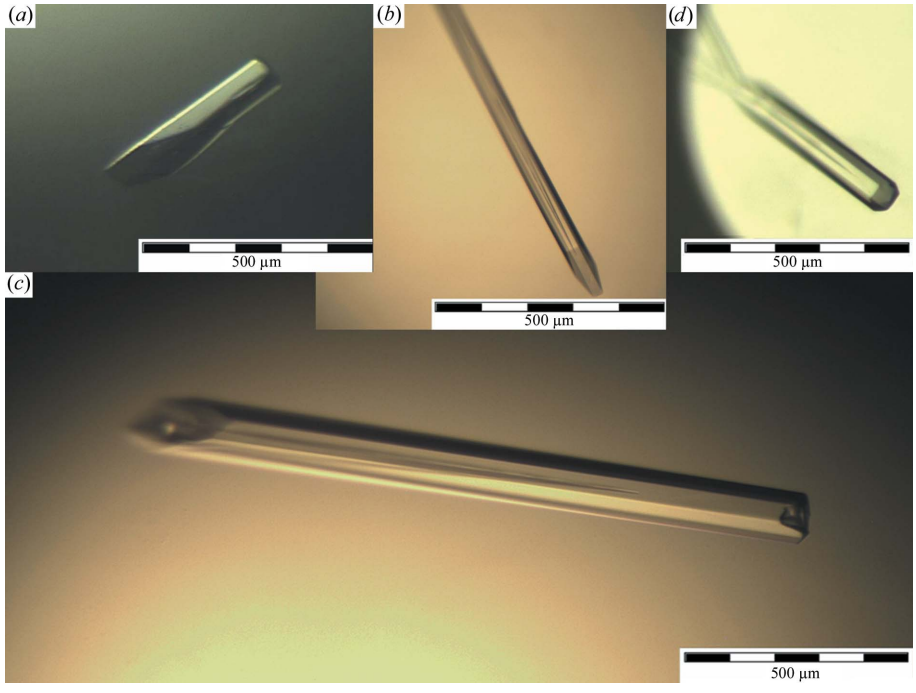

Figure 1
Single crystals of recombinant tomato nuclease R-TBN1. (*a*) Crystals grown in 3 d by microseeding using condition 1 (Table 1). (*b*) Crystals grown in a hanging drop in one week using condition 2 (Table 1). (*c*) Crystals grown in a hanging drop in one week using condition 3 (Table 1). (*d*) Crystals grown in microbatch in one week using condition 4 (Table 1).

Table 2
Data-collection and processing statistics for the rhombohedral crystal form of R-TBN1.

Values in parentheses are for the highest resolution shell. Crystal types are identified according to the crystallization conditions described in Table 1.

Crystal type and data set	Condition 2, SAD	Condition 3, peak, all images (1–720)	Condition 3, peak, images 1–360	Condition 3, inflection point
No. of crystals	1	1	1	1
X-ray source and end station	BL14.1, BESSY II	BL14.1, BESSY II	BL14.1, BESSY II	BL14.1, BESSY II
Detector	MAR Mosaic CCD 225	MAR Mosaic CCD 225	MAR Mosaic CCD 225	MAR Mosaic CCD 225
Wavelength (Å)	1.2782	1.2827	1.2827	1.2830
Space group	*H*3	*H*3	*H*3	*H*3
Unit-cell parameters (Å)				
$a = b$	115.8	115.9	115.7	116.5
c	75.2	75.3	75.2	75.5
Resolution range (Å)	30–3.60 (3.73–3.60)	45–3.20 (3.35–3.20)	45–3.20 (3.35–3.20)	45–3.60 (3.76–3.60)
Mosaicity range (°)	1.2–2.6	0.9–1.3	0.9–1.3	1.1–1.5
No. of measured reflections	24038	143035	72531	77989
No. of unique reflections	4304 (436)	6127 (749)	6219 (785)	4371 (557)
Completeness (%)	100.0 (100.0)	100.0 (100.0)	100.0 (100.0)	100.0 (100.0)
Average multiplicity	5.6 (5.1)	23.3 (23.3)	11.7 (11.3)	17.8 (17.7)
Mean $I/\sigma(I)$	18.3 (3.0)	44.7 (5.6)	30.7 (4.0)	36.3 (5.2)
$R_{\rm merge}$	0.104 (0.543)	0.092 (0.757)	0.074 (0.566)	0.102 (0.599)
$R_{\rm r.i.m.}$†	0.116 (0.621)	0.096 (0.795)	0.076 (0.576)	0.104 (0.638)
$R_{\rm anom}$‡	0.059 (0.259)	0.044 (0.158)	0.045 (0.163)	0.038 (0.146)
Overall *B* factor from Wilson plot (Å^2)	106.5	123.6	128.3	113.4

† $R_{\rm r.i.m.} = \sum_{hkl}[N/(N-1)]^{1/2}\sum_i |I_i(hkl) - \langle I(hkl)\rangle|/\sum_{hkl}\sum_i I_i(hkl)$ (Weiss, 2001). ‡ $R_{\rm anom} = \sum_{hkl} |I(hkl) - I(\bar{h}\bar{k}\bar{l})|/\sum_{hkl} \overline{I(hkl)}$ (Weiss, 2001).

The drop was formed by mixing 0.5 µl protein solution (at a concentration of 5 mg ml^{-1}) with 1.0 µl reservoir solution. The third condition was similar to the second and was created by replacing 4%(*v*/*v*) DMSO with 0.48 *M* hexane-1,6-diol. The best crystals (of approximate dimensions 1500 × 100 × 100 µm) from both conditions were obtained within one week (Figs. 1*b* and 1*c*). Crystals of suitable quality were also grown by microbatch crystallization under paraffin oil (the fourth condition). The crystallization drop was formed by mixing 0.5 µl protein solution (5 mg ml^{-1}) with 1.0 µl precipitant solution composed of 0.1 *M* bis-tris pH 6.5, 10%(*w*/*v*) PEG MME 5000 and 2%(*v*/*v*) butane-2,3-diol (Fig. 1*d*). The methods and precipitants that yielded the best crystals are summarized in Table 1. Chemicals were purchased from Hampton Research (Aliso Viejo, California, USA) and Sigma–Aldrich.

2.3. X-ray diffraction experiments and data collection

Crystals from all of the conditions mentioned above were equilibrated for 30–60 s in crystallization solution with glycerol added to 25%(*v*/*v*) concentration as a cryoprotectant and then mounted in 20 µm diameter nylon CryoLoops (Hampton Research) and quickly vitrified in liquid nitrogen. Preliminary diffraction analyses were performed using an in-house Gemini Enhanced Ultra diffractometer with an Atlas CCD detector (Oxford Diffraction). The crystals from condition 1 (see Table 1) belonged to the orthorhombic system (form *A*) and the crystals grown in conditions 2–4 belonged to the rhombohedral system (form *B*). Crystals of both forms diffracted very weakly with poor overall diffraction quality, which included anisotropy, strong diffuse scattering, low resolution and high mosaicity (Fig. 2). The effects of cryoprotectants at different concentrations and of different compositions on diffraction quality and diffraction experiments at room temperature were tested. A number of re-annealing experiments and post-crystallization treatments such as crystal dehydration and cross-linking with glutaraldehyde (pentane-1,5-dial) were performed (Heras & Martin, 2005). None of these approaches had a significant influence on the quality of the diffraction data and therefore ∼200 single crystals were tested in order to find suitable candidates for data collection. Data sets for structure analysis of both crystal forms were collected at 100 K on beamline BL14.1 at the BESSY II synchrotron-radiation source, Helmholtz-Zentrum Berlin using a MAR Mosaic CCD 225 detector and a mini kappa goniometer.

2.3.1. X-ray diffraction analysis of the orthorhombic crystal form

One ω-scan data set was collected from an orthorhombic crystal (form *A*) with parameters $\Delta\omega = 0.25°$, $\kappa = 0°$, $\lambda = 0.91841$ Å (13.4999 keV) and an exposure time per oscillation frame of 15 s. The crystal diffracted to 5.2 Å resolution, but owing to severe anisotropy of the diffraction only data to a 5.6 Å resolution limit could be used further. A total of 281 images were recorded and the diffraction intensity dropped rapidly during the experiment so that a complete data set could not be collected. The data were processed with *HKL*-2000 (Otwinowski & Minor, 1997). The Patterson symmetry of the

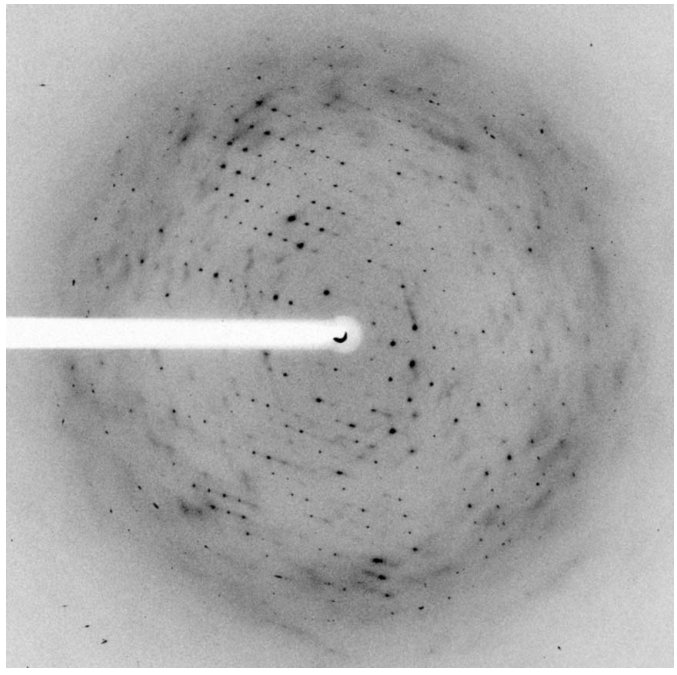

Figure 2
X-ray diffraction image of a rhombohedral crystal of R-TBN1 grown in condition 3 (Table 1), clearly showing high anisotropy and strong diffuse scattering. The pattern was recorded on BL14.1 at the BESSY II synchrotron-radiation source.

crystal is *Pmmm* and analysis of systematic absences revealed the presence of two screw axes (along the *a* and *b* directions). The presence of a screw axis along *c* could not be determined because of missing reflections. The space group of the orthorhombic form is therefore either $P2_12_12$ or $P2_12_12_1$, with unit-cell parameters $a = 383.2$, $b = 67.8$, $c = 113.6$ Å. Zinc ions are expected to be natively present in the protein and their presence was confirmed by analysis of an X-ray fluorescence spectrum (at $\lambda = 0.91841$ Å using a Bruker AXS/Roentec X-Flash XRF detector on BL14.1) and subsequently by an absorption-edge scan near the *K* line of zinc.

2.3.2. X-ray analysis of the rhombohedral crystal form. Data were collected from two rhombohedral (form *B*) crystals. One ω-scan was measured at $\lambda = 1.2782$ Å (slightly above the Zn *K* peak energy as derived from an absorption-edge scan) from a crystal obtained using condition 2 in Table 1 in order to maximize the measured anomalous differences. 180 oscillation images were recorded with an oscillation width $\Delta\omega = 1^\circ$, $\kappa = 0$ and an exposure time per frame of 10 s. The crystal diffracted to 3.6 Å resolution and belonged to space group *H*3.

A two-wavelength MAD data set was collected from a rhombohedral crystal obtained using condition 3 (Table 1). The first ω-scan was measured at the peak wavelength $\lambda_{peak} = 1.2827$ Å, with $\Delta\omega = 1^\circ$, $\kappa = 0^\circ$, an exposure time per frame of 12 s and a total of 720 oscillation images. 546 images were then recorded at the inflection-point wavelength $\lambda_{infl} = 1.2830$ Å, with $\Delta\omega = 1^\circ$, $\kappa = 0^\circ$ and an exposure time per frame of 3 s. The peak and inflection-point wavelengths were derived from an experimentally determined absorption-edge scan. The crystal diffracted to 3.2 Å resolution, but useful signal in the inflection-point data was limited to 3.6 Å resolution owing to radiation damage and the exposure time being reduced to achieve higher redundancy for MAD phasing. The data were processed using *HKL*-2000 (Otwinowski & Minor, 1997) and the statistics are summarized in Table 2. For MAD phasing trials only the first 360 images of the peak data set were used to avoid the inclusion of data that were strongly affected by radiation damage.

Crystals from condition 4 (Table 1) diffracted to lower resolution compared with those from conditions 2 and 3 and data were not collected in this case.

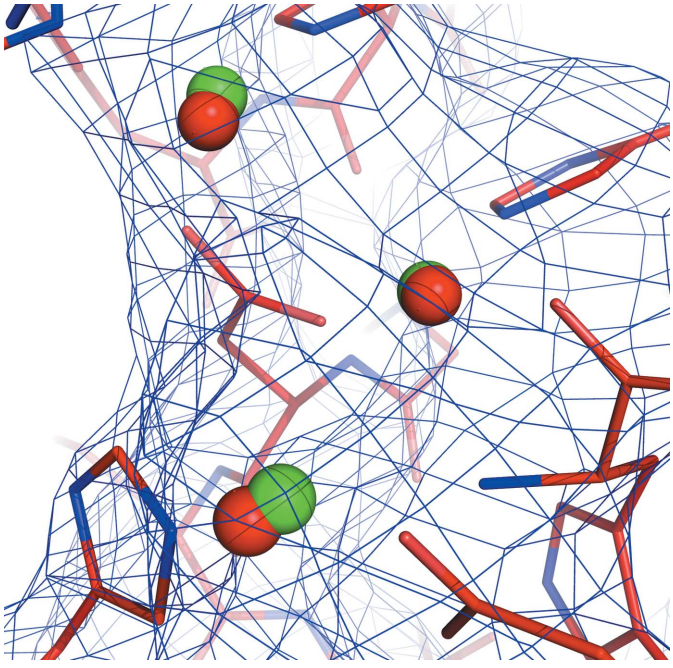

Figure 3
The Zn^{2+} cluster (red spheres) of P1 nuclease placed into the experimental electron-density map matched the three Zn^{2+} ions found by experimental phasing (green spheres). Residues of P1 nuclease are shown as sticks; positions of atoms correspond to the phased MR solution without any further refinement. The F_o, φ_{SHELXE} Fourier is contoured at the 1.3σ level. The graphics were created using *PyMOL* (DeLano, 2002).

3. Results and discussion

The crystals of both forms *A* and *B* are highly mosaic and provide anisotropic diffraction with intensive diffuse scattering. The effective maximal difference in the diffraction limit in different directions reaches 1 Å for the orthorhombic data sets and 0.4 Å for the rhombohedral data sets. Twinning was not indicated by any tools or statistics. According to Matthews coefficient calculations (Matthews, 1974), the asymmetric unit of the orthorhombic crystal (form *A*) contains eight ($V_M = 2.5$ Å^3 Da^{-1}) or nine ($V_M = 2.2$ Å^3 Da^{-1}) molecules of TBN1, while the rhombohedral form (form *B*) contains only one molecule ($V_M = 2.6$ Å^3 Da^{-1}).

Attempts to solve the phase problem for both forms by molecular replacement with the closest related nuclease of known structure, P1 nuclease from *P. citrinum* (PDB entry 1ak0; Romier *et al.*, 1998; 28% sequence identity), as a model were unsuccessful. The search was performed with the *MOLREP* program (Vagin & Teplyakov, 2010) from the *CCP*4 suite.

A MAD phase-problem solution was attempted using the first 360 peak images and the inflection-point data from the rhombohedral crystal using *SHELXC*, *SHELXD* and *SHELXE* (Sheldrick, 2008). It resulted in the location of three Zn^{2+} ions with occupancy factors above 0.4 (1.0, 0.96 and 0.44) and an expected geometrical arrangement similar to that observed for P1 nuclease. One of the enantiomorphs of the heavy-atom sets provided improved contrast and connectivity in the phase-modification step (original contrast 0.598, inverted contrast 0.539; original connectivity 0.816, inverted connectivity 0.800). The initial electron-density map phased by the original solution clearly showed separation of the solvent and protein regions as well as the positions of some α-helices, but direct model building (manual or automated) was not possible.

A preliminary structure model was built by placing the P1 nuclease structure into experimental electron density using *MOLREP* (Vagin & Teplyakov, 2010). A solution with an overall contrast of 7.45 was found and the Zn^{2+} cluster of P1 nuclease matched the three Zn^{2+} ions found by experimental phasing (Fig. 3). Rigid-body refinement of the initial model using *REFMAC*5 (Murshudov *et al.*, 1997) resulted in $R = 0.49$ and $R_{free} = 0.55$. Further model building and refinement were not possible owing to insufficient data quality.

Tomato bifunctional nuclease 1 N-glycosylated at three sites crystallizes and preliminary X-ray diffraction analysis confirmed the presence of three Zn^{2+} ions in the enzyme active site. Better crystals that provide diffraction data of higher quality are necessary for the successful structure determination of TBN1.

This project was supported by the Czech Science Foundation (projects 310/09/1407, 202/06/0757 and 521/09/1214) and by the EC under ELISA grant agreement No. 226716 (synchrotron-access funding, projects 09.2.90262 and 10.1.91347). We also gratefully acknowledge support from Praemium Academiae of AS CR, Institution Research Plan AVOZ10100521 of the Institute of Physics AS CR, Institution Research Plan MSM6046137305 of the Institute of Chemical Technology and the Grant Agency of Charles University, Prague (project 170710). The authors wish to thank Dr N. Darowski

of Helmholtz-Zentrum Berlin for support at beamline BL14.1 of BESSY II.

References

Aleksandrowicz, J. (1958). *Lancet*, **272**, 420.
Ardelt, W., Mikulski, S. M. & Shogen, K. (1991). *J. Biol. Chem.* **266**, 245–251.
Chang, S. C. & Gallie, D. R. (1997). *Plant Physiol.* **113**, 1253–1263.
Cudney, R., Patel, S., Weisgraber, K., Newhouse, Y. & McPherson, A. (1994). *Acta Cryst.* D**50**, 414–423.
D'Alessio, G., Floridi, A., De Prisco, R., Pignero, A. & Leone, E. (1972). *Eur. J. Biochem.* **26,** 162–167.
Dangl, J. L., Dietrich, R. A. & Thomas, H. (2000). *Biochemistry and Molecular Biology of Plants*, edited by B. Buchman, W. Gruissen & R. Jones, pp. 1044–1100. Rockville: American Society of Plant Physiology.
D'Arcy, A., Mac Sweeney, A., Stihle, M. & Haber, A. (2003). *Acta Cryst.* D**59**, 396–399.
Darzynkiewicz, Z., Carter, S. P., Mikulski, S. M., Ardelt, W. J. & Shogen, K. (1988). *Cell Tissue Kinet.* **21,** 169–182.
DeLano, W. L. (2002). *PyMOL.* http://www.pymol.org.
Dostál, J. & Matoušek, J. (1972). *J. Reprod. Fertil.* **31**, 273–275.
Gite, S. U. & Shankar, V. (1995). *Crit. Rev. Microbiol.* **21**, 101–122.
Green, P. J. (1994). *Annu. Rev. Plant Physiol. Plant Mol. Biol.* **45**, 421–445.
Heras, B. & Martin, J. L. (2005). *Acta Cryst.* D**61**, 1173–1180.
Hosokawa, S. & Irie, M. (1971). *J. Biochem.* **69**, 683–697.
Ledoux, L. (1955). *Nature (London)*, **176**, 36–37.
Lipovova, P., Podzimek, T., Orctova, L., Matousek, J., Pouckova, P., Soucek, J. & Matousek, J. (2008). *Neoplasma*, **55**, 158–164.
Matoušek, J., Kozlová, P., Orctová, L., Schmitz, A., Pešina, K., Bannach, O., Diermann, N., Steger, G. & Riesner, D. (2007). *Biol. Chem.* **388**, 1–13.
Matoušek, J., Orctová, L., Škopek, J., Pešina, K. & Steger, G. (2008). *Biol. Chem.* **389**, 905–918.
Matousek, J., Podzimek, T., Pouckova, P., Stehlik, J., Škvor, J., Lipovova, P. & Matousek, J. (2010). *Neoplasma*, **57**, 339–348.
Matousek, J., Podzimek, T., Poucková, P., Stehlík, J., Skvor, J., Soucek, J. & Matousek, J. (2009). *Oncol. Res.* **18**, 163–171.
Matthews, B. W. (1974). *J. Mol. Biol.* **82**, 513–526.
Murshudov, G. N., Vagin, A. A. & Dodson, E. J. (1997). *Acta Cryst.* D**53**, 240–255.
Olson, B. H., Jennings, J. C., Roga, V., Junek, A. J. and Schuurmans, D. M. (1965). *Appl. Microbiol.* **13**, 314–321.
Otwinowski, Z. & Minor, W. (1997). *Methods Enzymol.* **276**, 307–326.
Pérez-Amador, M. A., Abler, M. L., DeRocher, J., Thompson, D. M., van Hoof, A., LeBrasseur, N., Lers, A. & Green, P. J. (2000). *Plant Physiol.* **122**, 169–180.
Romier, C., Dominguez, R., Lahm, A., Dahl, O. & Suck, D. (1998). *Proteins*, **32**, 414–424.
Sheldrick, G. M. (2008). *Acta Cryst.* A**64**, 112–122.
Soucek, J., Skvor, J., Poucková, P., Matousek, J., Slavík, T. & Matousek, J. (2006). *Neoplasma*, **53**, 402–409.
Vagin, A. & Teplyakov, A. (2010). *Acta Cryst.* D**66**, 22–25.
Weiss, M. S. (2001). *J. Appl. Cryst.* **34**, 130–135.